CARBON 80 (2014) 808–822

Available at www.sciencedirect.com

ScienceDirect

journal homepage: www.elsevier.com/locate/carbon

On the use of new oxidized Co–Cr–Pt–O catalysts for vertically-aligned few-walled carbon nanotube forest synthesis in electron cyclotron resonance chemical vapor deposition

I-Ju Teng [a,b], *Chong-Sian Huang* [c], *Hui-Lin Hsu* [d], *I-Chuan Chung* [e], *Sheng-Rui Jian* [b,*], *Nazir P. Kherani* [d], *Cheng-Tzu Kuo* [c], *Jenh-Yih Juang* [a,f]

[a] *Centre for Interdisciplinary Science, National Chiao Tung University, Hsinchu 30010, Taiwan*
[b] *Department of Materials Science and Engineering, I-Shou University, Kaohsiung 84041, Taiwan*
[c] *Department of Materials Science and Engineering, National Chiao Tung University, Hsinchu 30010, Taiwan*
[d] *Department of Electrical and Computer Engineering, University of Toronto, Toronto M5S3G4, Canada*
[e] *Center for Nano Science and Technology, National Chiao Tung University, Hsinchu 30010, Taiwan*
[f] *Department of Electrophysics, National Chiao Tung University, Hsinchu 30010, Taiwan*

ARTICLE INFO

Article history:
Received 11 April 2014
Accepted 12 September 2014
Available online 19 September 2014

ABSTRACT

A new class of the multi-element catalysis system, Co–Cr–Pt–O, is used for vertically-aligned few-walled carbon nanotube (CNT) forest synthesis by a sandwich-growth technology in electron cyclotron resonance chemical vapor deposition. The effect of catalyst compositions on the resulting particle sizes after pretreatment, and the influence of process parameters on the CNT forest heights and diameters are investigated. Results show that a plasma pretreatment step reduces the metal oxides present in the as-deposited Co–Cr–Pt–O catalyst to their metallic states or to mixed metallic/oxidic states, and the co-catalytic synergistic effect during the reduction process thus leads to the production of uniformly small particles with a size of 3.3–3.9 nm over the substrate. Moreover, with CH_4 as the carbon source, vertically-aligned CNT forests of ~12 μm in height are achieved, and further characterizations indicate that the forests consist of dominant triple-walled nanotubes with an average inner tube diameter of 3.2–3.7 nm mostly. Additionally, field emission measurements show that the turn-on field of the CNT-forest emitters is below 2.6 V/μm, and the emission current density can reach 110 mA/cm^2 at 4.5 V/μm. High reproducibility of field emission characteristics and Raman signals suggests the regularity of the CNT forests in structure and size.

© 2014 Elsevier Ltd. All rights reserved.

1. Introduction

Carbon nanotubes (CNTs) in the form of vertically-aligned forests possess many structure advantages compared to bulk CNT powders or randomly-oriented CNT mats, making them attractive candidates for a wide range of multifunctional applications. For example, vertical assemblies of CNT forests can provide a large well-defined surface area and a mesopor-

* *Corresponding author.*
E-mail address: srjian@gmail.com (S.-R. Jian).
http://dx.doi.org/10.1016/j.carbon.2014.09.040
0008-6223/© 2014 Elsevier Ltd. All rights reserved.

ous structure, permitting enhanced interaction and functionality among nanotubes, and therefore advancing the developments of sensitive sensing devices [1,2] and flexible supercapacitor electrodes [3–5] as well. Besides, the aligned growth can produce vertical CNTs with fairly uniform height and a very narrow diameter distribution, making it possible to use as field emitters in panel display [1,2]. Further, forests of vertically-aligned CNTs with a high density can result in more conduction channels per unit area for electrons and heat along the tubes, which is critical for potential use in electronic interconnects and thermal management [6–9]. Applications of CNT forests are also extended to macroscopic scales, such as nanotube yarn- and sheet-based lightweight data cables, electromagnetic shielding materials, polarized light sources, polymer welding, flexible touch screens, incandescent display, transparent loudspeaker, transmission electron microscopy nanogrids, artificial muscles, or underwater sound generators [6,10–13]. These emerging CNT applications can be attributed to the discovery of continuous dry-drawn CNT yarns by Fan group in 2002 [14], and then to the focus of intense research efforts to exploit new organizational structures and capabilities [10–13]. Organized CNT architectures prepared by drawing or spinning of CNT forests into self-assembled yarns or sheets offer advantages not only of scaling up the interesting physico-chemical properties of individual CNTs and reducing the cost of CNT based products, but also of realizing new functionalities and opening up novel application areas [6,10–14]. The facts mentioned above reveal that aligned CNTs in a forest-like morphology are thus promising for various applications in many fields and, the vertical orientation of nanotubes to the substrate surface can offer significant performance advantages and achieve commercial viability.

There are many synthesis techniques available for forest-like vertically-aligned CNTs, in which chemical vapor deposition (CVD) is particularly attractive as it offers many control parameters and allows for an effective integration of various CNT forests with different characteristics into certain useful devices [1,10]. It is generally accepted that in CVD process for the synthesis of CNT forests, types of catalysts, buffer layers, carbon feedstocks, as well as various growth conditions can lead to CNT growth variation. Among all process parameters, the size and the number density of catalyst particles produced on the substrate before growing CNTs are surely critical to determine the diameter and the density of resultant nanotubes in a forest. It is being considered important because these structural features are expected to have significant influences on some commercial applications domain of CNT forests [15–19]. Due to these reasons, many efforts in recent years have been focused on optimizing the catalysts used in the growth [8,19–23], or on developing a new class of catalyst systems [24–27] for growing wall-number-selected CNT forests with maximum length, density, and favorable alignment and geometry. So far, in addition to the common iron-group metals (iron, cobalt, nickel), some metal oxides [24], mixed metal oxides [25], binary metals [26], and triple-layer thin films [27], have been experimentally demonstrated to exhibit high activity in catalyzing the growth of high-yield CNT forests. Accordingly, it promotes the motivation for exploring new catalysts for CVD growth of forest-like CNT arrays. Moreover, investigations of different types of catalysts used and various parameters involved in CVD processes provide not only more chance to understand the relationship between the catalyst compositions and the resultant CNT growth, but also the important insight into rational design of new catalyst systems enabling the CVD synthesis of CNTs. These therefore give the possibilities to fine-control over the characteristics of as-grown CNT forests. Accordingly, in this paper we will explore the possibility of using a new type of Co-based oxide species as the catalyst to promote few-walled CNT forest growth by CVD, and further investigate the effect of growth conditions on the final nanostructure morphologies to open new perspectives both for rational catalyst design and for structural control of vertically-aligned CNTs.

In this work, we report on the use of a new multi-element catalysis system, Co–Cr–Pt–O, for sandwich growth of vertically-aligned few-walled CNT forests in electron cyclotron resonance chemical vapor deposition (ECRCVD). The remarkable capability of the newly-developed oxidized catalyst to produce densely-packed small particles during pre-growth stage known as pretreatment is highlighted. The growth behavior of the CNT forests by varying the substrate preheating temperature, operating pressure, substrate bias, CH_4/H_2 ratio, and plasma power is also systematically investigated and compared. Lastly, the readily available CNT forests are used as cathode materials for electron field emission without any post-treatment, and results show a stable and reproducible emission performance for the fabricated CNT-forest emitters.

2. Experimental

A newly-developed oxidized catalyst of Co–Cr–Pt–O with 2 nm thickness was directly deposited onto Si wafers by reactive direct current sputtering. The Si wafers were precleaned in an ultrasonic bath with acetone, isopropanol, and deionized water for 15 min in each liquid followed by careful blow-drying with a nitrogen gun before being loaded into the sputtering chamber. A Co–Cr–Pt alloy target (Co: 57.08 at%, Cr: 10.97 at%, Pt: 31.95 at%) was employed for reactive sputtering. The sputtering chamber was initially evacuated to a base pressure of less than 10^{-4} Pa and then pre-sputtering of 20 min was carried out in a pure Ar ambient at a constant flow rate of 30 sccm and a sputter pressure of $\sim 10^{-1}$ Pa to remove any contaminants and/or impurity on the target surface. After pre-sputtering, a mixture of Ar/O_2 with a fixed flow ratio of 10/30 sccm/sccm was introduced through mass flow controllers to keep a working pressure of $\sim 10^{-1}$ Pa. The purity of the gases was 99.9995% in each case. The thickness of the Co–Cr–Pt–O layer was controlled from 0.5 to 20 nm by the deposited rate determined transmission electron microscopy measurement of a test Co–Cr–Pt–O film deposited in a known time. Catalyst layer thicknesses were determined using a combination of X-ray photoelectron spectroscopy and atomic force microscopy techniques.

Catalyst pretreatment followed by CNT growth was performed in an ECRCVD system, in which a sandwich-like substrate stack configuration shown in Fig. 1(a) was utilized to prevent the catalyst from being directly exposed to the

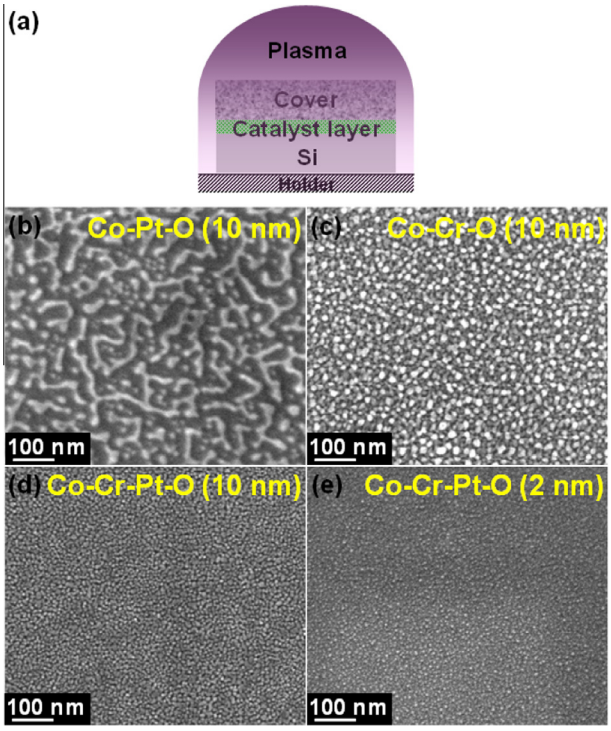

Fig. 1 – (a) Schematic illustration of the sandwiched specimen stack structure used in this work for vertically-aligned CNT forest synthesis in ECRCVD. (b–e) SEM images of 10 nm Co–Pt–O, Co–Cr–O, and Co–Cr–Pt–O, and 2 nm Co–Cr–Pt–O deposited on Si wafers after being heated to ~560 °C in an ECRCVD system, and then followed by a 10^{-1} Pa hydrogen plasma pretreatment with a flow rate of 50 sccm, plasma power of 560 W, and substrate bias of −30 V for 10 min. (A color version of this figure can be viewed online.)

plasma so that severe ion bombardment of the growing surface can be suppressed. The catalyst-coated substrates were first heated to ~560 °C and then pretreated by hydrogen plasma at ~10^{-1} Pa pressure, with a hydrogen flow rate of 50 sccm, plasma power of 560 W, and substrate bias of −30 V for about 10 min to produce nanoparticles for subsequent growth of CNTs. In order to examine the correlation between different combinations of the cobalt-based oxide catalysts and the resulting particle sizes after pretreatment, oxidized Co–Pt–O and Co–Cr–O layers deposited on Si wafers were also employed as reference samples during the pretreatment process for comparison. The subsequent growth of CNTs was carried out from the oxidized Co–Cr–Pt–O catalyst under the CH_4/H_2 environment for 45 min. The substrate preheating temperature (350–680 °C), operating pressure (10^{-1}–10^3 Pa), negative substrate bias (30–400 V), CH_4/H_2 ratio (1/50–50/50 sccm/sccm), and plasma power (115–750 W) were varied to evaluate their effects on the as-synthesized CNT forest heights and the average diameter of the nanotubes in each forest.

The morphology and microstructure of the obtained catalyst particles and CNTs were examined by scanning electron microscopy (SEM, JEOL-6500; FEI Nano SEM, Nova 200) and transmission electron microscopy (TEM, JEOL JEM-2100). Energy dispersive X-ray spectrometry (EDS) coupled to SEM and TEM was applied to identify the elemental compositions of the as-grown CNT forest samples and individual catalyst particles before and after the CNT forest growth process. X-ray photoelectron spectroscopy (XPS, VG Scientific, Microlab 350) was employed to characterize the bonding energy, chemical state, and composition distribution along the depth of the Co–Cr–Pt–O catalyst in the as-deposited state and after hydrogen plasma pretreatment. The degree of graphitization of the CNT-grown samples was further determined by micro-Raman spectroscopy (Renishaw RM-1000) with an excitation of 514.5 nm. To obtain averaged spectra, for each sample, more than five different locations were examined by Raman spectroscopy using an approximately 5 μm diameter laser spot. The field emission properties of the CNT forests were measured in a vacuum chamber at a pressure of less than 10^{-4} Pa using a simple diode configuration. The distance between the anode and the emitting surface was kept at ~200 μm defined by a precision screw meter, and the effective emission area was about 3.2 mm^2. A Keithley 237 high-voltage source-measure unit was utilized to supply the voltage between the electrodes and to collect the emitted current.

3. Results and discussion

It is known that densely-packed small catalyst particles after pretreatment are generally required for aligned growth of single or few-walled CNTs by CVD method. Therefore, we investigate in the first part the effect of catalyst compositions on the resulting particle sizes after hydrogen plasma pretreatment. Here, Si wafers, respectively, coated with 10-nm-thick Co–Pt–O, Co–Cr–O and Co–Cr–Pt–O layers, and 2-nm-thick Co–Cr–Pt–O layer are subject to hydrogen plasma pretreated for 10 min at a hydrogen flow rate of 50 sccm, plasma power of 560 W, substrate bias of −30 V, operating pressure of ~10^{-1} Pa, where the substrate temperature can be increased to ~595 ± 5 °C by plasma heating, as shown in Fig. 1(b–e). One can see that after pretreatment the Co–Pt–O layer becomes discontinuous with a broad distribution of particle/island sizes (Fig. 1(b)), while the particles obtained from the Co–Cr–O catalyst reveal a relatively uniform size, as displayed in Fig. 1(c). However, the Co–Cr–Pt–O layer, pretreated by this process, gets broken into particles with apparently smaller sizes and greater density than those obtained from the Co–Pt–O and Co–Cr–O layers. Moreover, as its thickness decrease from 10 to 2 nm, both the as-produced nanoparticle size and size distribution are reduced, as shown in Fig. 1(d and e). The results indicate that in our performed experiments the addition of Cr and Pt to the Co-based oxide catalysts can induce the production of extremely small and uniformly distributed particles after a plasma pretreatment step. In the case of sufficiently small catalyst particles created aligned growth of CNT forests with a rather small diameter and narrow diameter distribution is thus favored. The promoting effect of Cr and Pt in the oxidized Co–Cr–Pt–O catalyst will be discussed further in the following sections. Since the multi-element catalysis system, Co–Cr–Pt–O (2 nm), tends to produce densely-packed small catalyst particles during the plasma

pretreatment, hereinafter, the behavior and chemical profiling of the catalysts, the factors affecting the surface morphology created, the optimized conditions to grow vertically-aligned few-walled CNT forests, as well as the CNT structural and electronic properties are analyzed only for those form on the Co–Cr–Pt–O (2 nm)/Si substrates.

The corresponding cross-sectional TEM images and EDS analysis of the catalyst particles displayed in Fig. 1(e) are shown in Fig. 2. It can be seen from Fig. 2(a) that the nanoparticles are uniformly distributed on the native oxide surface of the silicon wafer, and are well separated from their nearest neighbors. The average diameter of the nanoparticles is estimated to be about 3.3–3.9 nm on the basis of counting more than 100 individual particles via TEM analysis. High-resolution TEM (HRTEM) further reveals good crystallinity of the nanoparticles (Fig. 2(b)). EDS analysis of these nanoparticles (Fig. 2(c)) shows the presence of O, Co, Cr, Pt, Si, and Cu. The O signal should be attributed to the oxidized species in the nanoparticles and/or the oxygen present in the substrate native oxide, and the Si signal should be due to the substrate effect. The Cu signal observed in the EDS spectrum comes from the TEM copper grid.

In order to understand the chemical information of these nanoparticles, we perform XPS to examine the differences in the bonding energy, chemical state, and composition distribution along the depth of the oxidized Co–Cr–Pt–O catalyst before and after pretreatment. Detailed XPS measurement results of the oxidized Co–Cr–Pt–O catalyst in the as-deposited state and after hydrogen plasma pretreatment are shown in Fig. 3. In each case, the spectra are calibrated to a charge reference of adventitious carbon with a core level binding energy of 284.6 eV, and for curve fitting we use published values of binding energies and a Shirley background [28]. The XPS spectra given in Fig. 3 show that in the case of the as-deposited sample (top curves) all components are in oxidized forms. In the Co 2p core level spectrum, two main peaks located at about 780.8 and 796.5 eV are assigned to Co 2p3/2 and Co 2p1/2, respectively. The Co 2p3/2 peak can be deconvoluted into two peaks centered at 780.15 and 781.39 eV, which can be attributed to the oxidation states of cobalt species (CoO and $CoSiO_x$). In the Cr 2p spectrum, the peaks corresponding to the Cr 2p3/2 and Cr 2p1/2 are observed at around 577.4 and 587.1 eV. The Cr 2p3/2 peak at 577.4 eV can be deconvoluted into three peaks centered at 576.37, 577.54, and 578.66 eV, suggesting the existence of chromium oxide species (Cr_2O_3 and CrO_x). In the Pt 4f spectrum, the couple of peaks at around 74.17 and 77.46 eV correspond to the Pt 4f7/2 and Pt 4f5/2, respectively. The Pt 4f7/2 peak can be fitted with two major peaks centered at binding energies of 73.92 and 74.79 eV, which can be assigned to PtO_x species. The presence of oxygen peaks between 529.83 and 532.88 eV gives additional confirmation for the existence of metal oxides in the sample. However, in the case of the hydrogen plasma-pretreated sample (the bottom curves of Fig. 3), it can be observed that the metal oxides present in the as-deposited Co–Cr–Pt–O catalyst are reduced to their metallic states and/or to a mix of metal and metal oxide systems. The dominant Co 2p3/2 peak at 778.18 eV can be associated to metallic Co. The Pt 4f7/2 region also shows a metallic component at 70.95 eV. Whereas the Cr remains in its oxidized form with

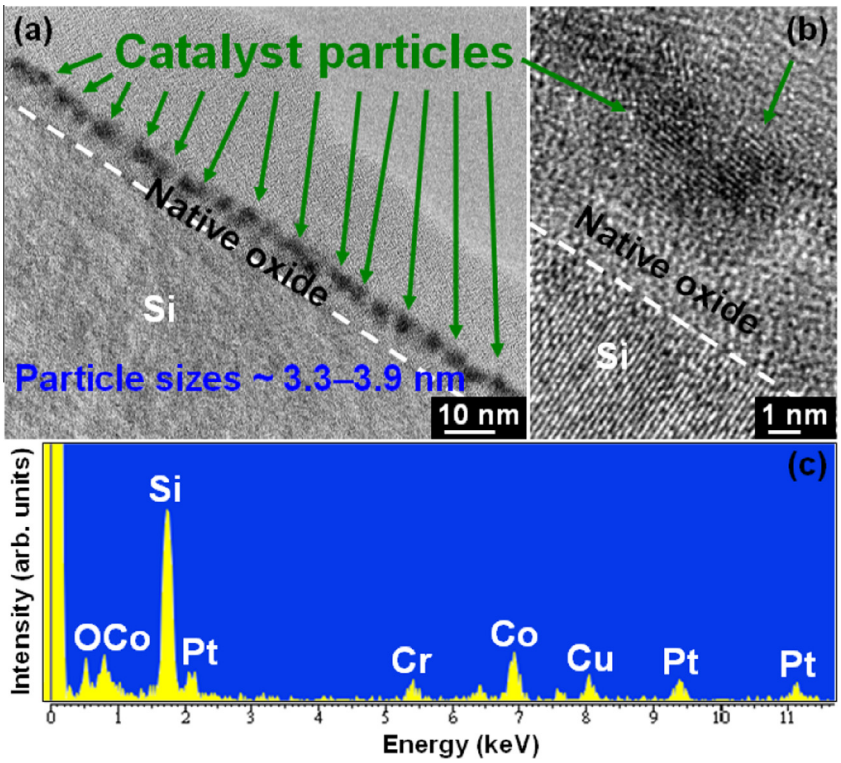

Fig. 2 – (a) TEM and (b) HRTEM images, and (c) EDS spectrum of the resulting catalyst particles after 10 min hydrogen plasma pretreatment on Co–Cr–Pt–O (2 nm)/Si substrates. (A color version of this figure can be viewed online.)

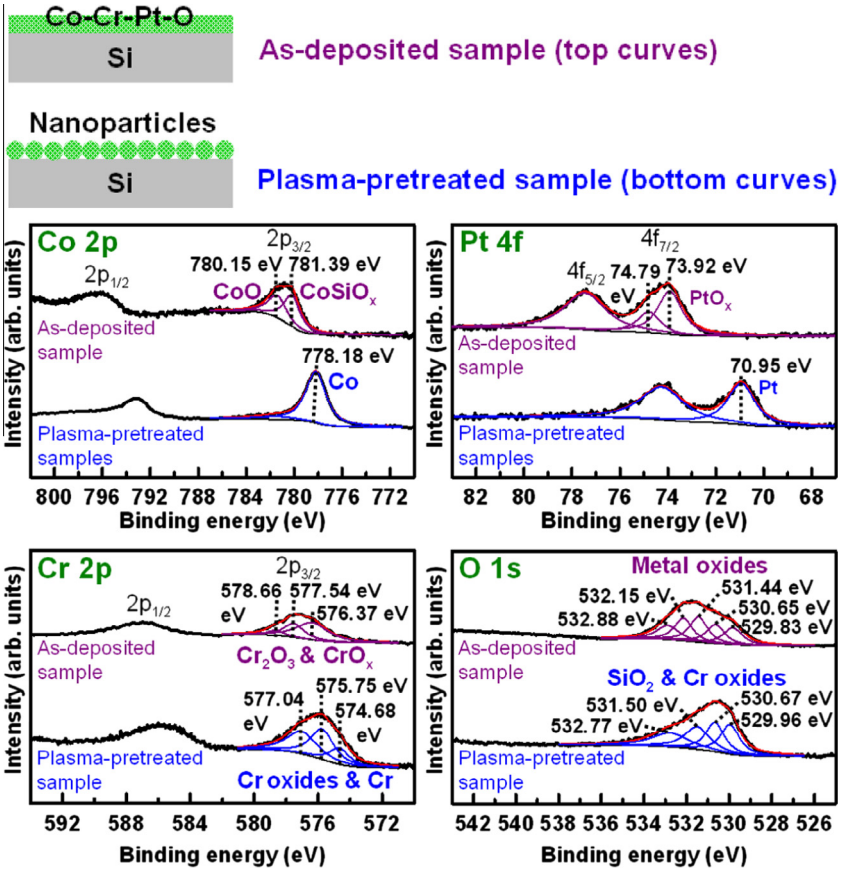

Fig. 3 – XPS spectra of Co 2p, Cr 2p, Pt 4f, and O 1s with curve fittings for the oxidized Co–Cr–Pt–O catalyst in the as-deposited state (top curves) and after hydrogen plasma pretreatment (bottom curves). (A color version of this figure can be viewed online.)

the 2p3/2 peaks between 575.75 and 577.04 eV, presumably mixed with partially reduced Cr metal (574.68 eV). A corresponding relationship can also be observed in the O 1s spectrum that shows peaks at binding energies between about 529.96–531.50 eV for chromium oxides. All the peak positions closely match the standard results in the Handbook of X-ray Photoelectron Spectroscopy [28]. The XPS measurements indicate that the potential benefit of the oxidized Co–Cr–Pt–O catalyst is the reduction of the metal oxides present in the as-deposited sample during the hydrogen plasma pretreatment to result in the production of extremely small and uniformly distributed catalyst particles, while the particles remain in good dispersion without coalescing into larger agglomerates. That is to say, after hydrogen plasma pretreatment the initial cobalt oxide species can be reduced to active cobalt metal particles which are the known effective catalyst species for the CVD growth of CNTs. Furthermore, with respect to the function of Cr in a mixed metallic/oxidic state obtained after a plasma pretreatment step, it can be deduced that, from the reports by Shaijumon et al. [29] and Bult et al. [30], the mixed chromium species can play the role as a stable passivation diffusion barrier in stabilizing the reduced particles in dispersion and preventing agglomeration and aggregation of individual particles. Such assumption can be further supported by the SEM images shown in Fig. 1(b–d), where well-defined particles instead of large particle agglomerates/aggregates can be obtained when Cr is added as a co-catalyst composition. Moreover, in the case of Pt species the reduction and/or decomposition of the platinum oxide through a thermal/plasma process are described in various studies. In good agreement with these results [31–35], we find that during pretreatment of the oxidized Co–Cr–Pt–O catalyst by hydrogen plasma, a special reductive decomposition process of PtO_x to Pt and O_2 due to thermal decay facilitates the production of very fine metallic platinum nanoparticles in our case. One consistent trend that can be also observed in Fig. 1(b–d) is that much smaller nanoparticles are created in the cases of catalysts with Pt content after pretreatment. The above results demonstrate the feasibility of our oxidized Co–Cr–Pt–O catalyst to produce tiny particles with homogeneous sizes around 3.3–3.9 nm after pretreatment, which is considered to be beneficial for the growth of aligned CNTs in forest-like uniform arrays with fewer walls and a narrow tube size distribution.

Longitudinal compositions of the catalyst-coated substrates before and after pretreatment are characterized by XPS with an etching depth about 2 nm, and the results are summarized in Table 1. It is observed that the oxygen concentration of samples dramatically decreases after hydrogen plasma pretreatment, whereas the atomic percentages of the Co, Cr, and Pt elements in the plasma-pretreated sample increases around 65%, 29%, 74%, respectively. These results

Table 1 – The atomic concentrations of the elements O, Co, Cr, Pt, and C present in the target, as-deposited sample, and plasma-pretreated sample, obtained from XPS analysis with an etching depth about 2 nm.

Elements (at%)	O	Co	Cr	Pt	C
Target	–	57.08	10.97	31.95	–
As-deposited sample	50.08	37.66	5.41	5.66	1.18
Plasma-pretreated sample	14.94	62.16	6.97	9.83	6.10

are in agreement with the XPS spectra shown in Fig. 3 that after exposure to hydrogen plasma, the Co and Pt are reduced from the oxide states to metallic Co and Pt clusters, while the chemical state of the plasma-pretreated Cr is probably mixture of metal and oxide.

Subsequent CNT growth steps with H_2 and CH_4 gases are performed using the plasma-pretreated sample shown in Fig. 1(e). In order to establish a relationship between the growth conditions and the resultant CNT forests, in the second part of this study, we analyze the influence of substrate preheating temperature, operating pressure, substrate bias, CH_4/H_2 ratio, and plasma power on the CNT forest heights and the average tube diameters (which is estimated from SEM images recorded at magnifications of greater than 250,000× of measuring over 100 CNTs grown at each set of processing conditions), while keeping the deposition time of 45 min. Fig. 4(a) shows the height and diameter dependence of the ECRCVD-synthesized CNTs on the substrate preheating temperature, in which the insets show the top-view SEM images of the CNT forests synthesized at 560, 590, and 680 °C, respectively. It should be noted that the final substrate temperature can increase approximately 30 ± 10 °C higher than the set temperature by averaging the steady-state growth due to the heating effect of the plasma. As shown, when the substrate preheating temperature is below 460 °C, the CNT forest heights remains below 100 nm, with an average tube diameter of about 8.1 ± 0.5 nm. However, above 510 °C a rapid increase in the CNT forest heights and a significant enhancement in vertical alignment are observed for small increases of the substrate preheating temperature. For example, the average height of the CNT forests for the substrate preheated to 510 °C is about 4 μm, while to 560 °C the forest height reaches almost 12 μm. Moreover, we observe that the variation in the CNT forest heights is smaller than 3% for the substrate preheating temperatures between 560 and 680 °C, suggesting that the average height of the CNT forests reaches a plateau at about 560 °C under the applied growth condition. Further, we find that between 460 and 560 °C, a decrease of average tube diameter with increasing temperature is found, while for higher temperatures of 560–680 °C, the average diameter of the CNTs in the forests tends to be around 5.1–5.3 nm with significantly good size uniformity between the forests grown in this temperature range. We consider that the main reason for the diameter reduction is probably due to the decrease of catalyst particle sizes, particularly between 560 and 680 °C, a special reductive decomposition process during pretreatment as mentioned in the above paragraph contributes to the production of sufficiently small and catalytically active particles, whose size in turn determines the CNT diameter and growth uniformity. Although a further increase of the substrate preheating temperature from 560 to 590 °C or to 680 °C gives rise to the CNT forests with similar heights and tube diameters, the CNT "fused" regions on the top end of the forests, which is similar to the top crust of entangled nanotubes on the vertically-aligned CNT forests of Zhang et al. [36], are obviously increased for the 590 and 680 °C samples, as indicated by the arrows in the insets of Fig. 4(a). Several previous studies have also shown similar SEM images that evidence the presence of an entangled crust structure at the top of CNT forests [37,38]. The formation of the top crusts is due to the self-organization of individual CNTs and/or CNT pillars in a forest at the early stages of a growth process [36–38]. Further experiments are being performed to understand the formation and influence of the entangled crusts residing on top of the CNT forests obtained by our ECRCVD plasma system. Concerning the height of the CNTs increases with increasing the substrate temperature, it is generally accepted that a higher temperature on the catalyst surface resulting from a higher substrate temperature can enhance the dissolving, diffusing and precipitating rates of carbon species through catalyst particles. Consequently, the growth rate of CNTs will increase and as-synthesized CNT yield will become larger within a certain period of deposition time [39,40]. On the basis of the above statement, we suggest that for the substrate temperature lower than ~500 °C during the steady growth in our case, the result of no observable or low-yield nanotubes is caused by the low dissolution and diffusion rates of carbon species required for graphite-like structure precipitation to form CNTs [41]. A further increase of the substrate temperature gives rise to the increase in the amount of dissolved carbon species and their diffusion rate, leading to significantly enhanced CNT growth [41], as observed in the cases of the CNT forests synthesized at the substrate preheating temperature of 510–680 °C. This part of the study demonstrates that CNT forests with an uniform height close to 12 μm can be synthesized by our ECRCVD using an oxidized Co–Cr–Pt–O catalyst in the substrate preheating temperature range of 560–680 °C. Although a maximum nanotube height is obtained at 680 °C, the temperature of 560 °C is the optimum one for the synthesis of the smallest-diameter CNT forests with less aggregation of tube ends, and is therefore being selected for the following experiments.

The operating pressure in an ECRCVD chamber is one of the important factors in determining the aligned growth of CNT forests. Fig. 4(b) shows the variation in the height and diameter of CNT forests with the operating pressure. It can be observed that there is almost no growth at 10^{-1} Pa, whereas at 10^{0} Pa the height and diameter of the CNT forests are about 0.7 μm and 9.2 ± 1.5 nm, respectively, indicating a

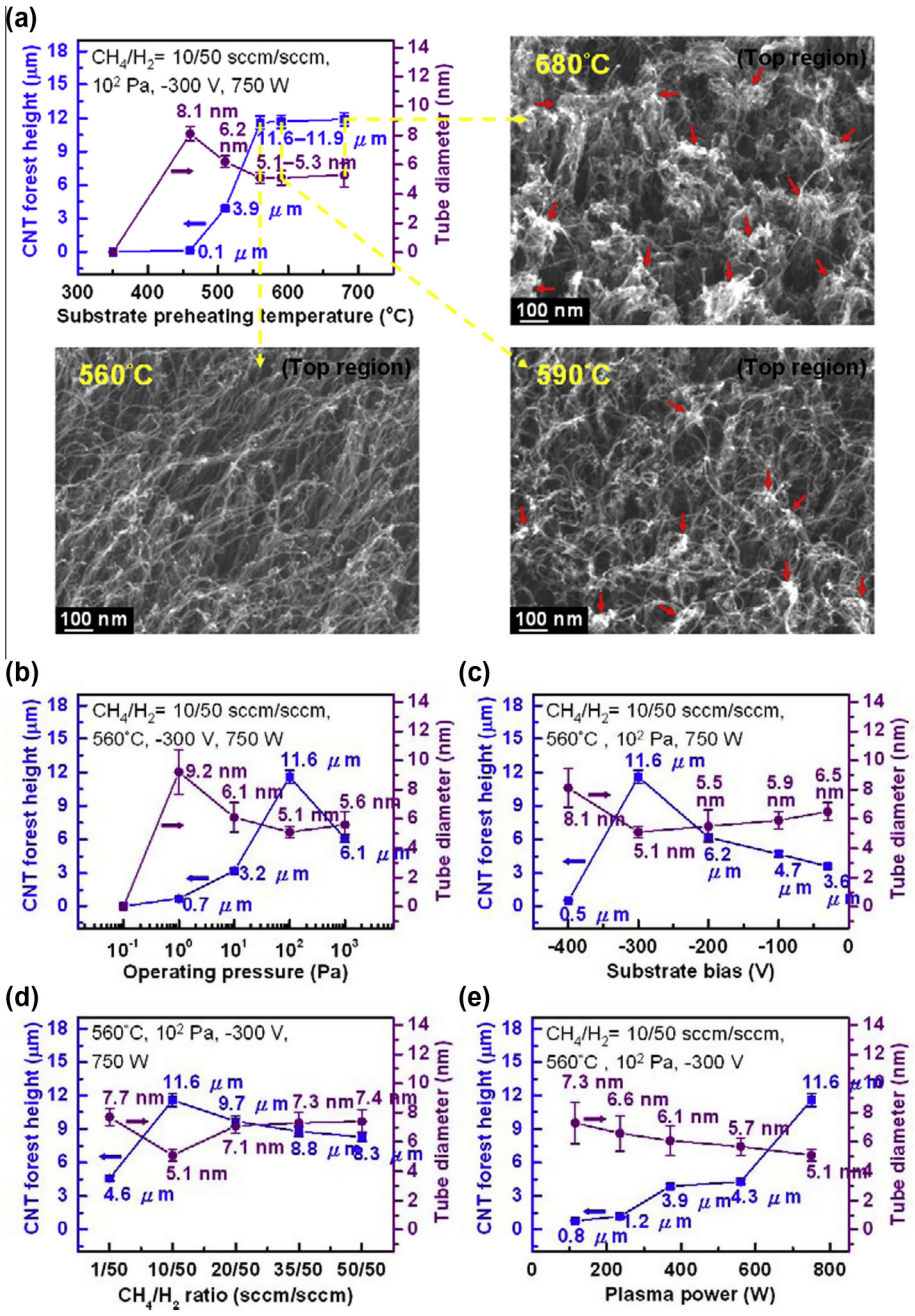

Fig. 4 – Plots showing the influence of (a) substrate preheating temperature, (b) operating pressure, (c) substrate bias, (d) CH_4/H_2 ratio, and (e) plasma power on the CNT forest heights and diameters, with ECRCVD process time fixed to 45 min. The insets in (a) show the top-view SEM images of the CNT forests synthesized at 560, 590, and 680 °C, respectively, and the arrows indicate the CNT "fused" regions on the top end of the forests. (A color version of this figure can be viewed online.)

slow increase in the CNT forest heights and the generation of larger diameter nanotubes at relatively low operating pressures. Furthermore, when the operating pressure is increased to 10^1 Pa the CNT forest height increases correspondingly to 3.2 μm with a decrease in the average tube diameter of 6.1 ± 1.0 nm. Further increasing the operating pressure to 10^2 Pa gives rise to a dramatic increase in the CNT forest height to 11.6 μm, while the mean diameter of nanotubes becomes smaller to 5.1 ± 0.4 nm. However, as the operating pressure is raised from 10^2 to 10^3 Pa, the height of the CNTs decreases down to 6.1 μm, wherein the nanotubes have an average diameter of about 5.6 ± 0.9 nm. It is known that when the operating pressure decreases, the number density of CH_4 molecules decreases, which reduces the probability of their reaction with the catalyst particles [39,42–44]. Consequently, no/fewer CNTs are generated at a low operating pressure, as occurred for the cases of 10^{-1}–10^0 Pa. With an increase of the operating pressure from 10^0 to 10^2 Pa there is a considerable increase in the CH_4 density, as a result, the number of collisions between reaction products and the catalyst surface

is increased, leading to more catalyst particles becoming activated within a certain period of deposition time. This therefore promotes greater nucleation and growth of CNTs, and thus resulting in the generation of CNTs with a relatively high yield as vertically-aligned forests [39,42–44]. Nevertheless, beyond this value (such as 10^3 Pa), the concentration of the reaction products during the growth process is too high and the dissolving rate is likely to be higher than diffusing and precipitating rates, giving rise to the saturated coverage of carbon species on the surface of activated catalyst particles. This saturation suppresses the catalytic activity of the particles and thus the yield/height of the CNTs is reduced [39,42–44]. Despite the changes in height, however, slight differences in the mean diameter of the nanotubes (5.1–6.1 nm on average) are observed at gas pressures between 10 and 1000 Pa. The investigations of the effect of operating pressure on the CNT forest growth process provide useful information in designing ECRCVD processes for manipulating the average height of as-synthesized CNT forests with good uniformity on diameter for various desired device applications.

In order to grow vertically-aligned CNT forests, in an ECRCVD plasma system the bias is always applied on the substrate. It is known that by applying a negative bias to a Si substrate, the substrate potential can be changed, and thus the energy of ion species landing on the catalyst surface will be changed, which further results in the variation of the growth rate and number density of carbon products [45]. Accordingly, investigations on the CNTs synthesized at various substrate biasing will be of interest. Fig. 4(c) shows the effect of the negative substrate bias on the CNT forest heights and diameters. The height of the CNTs increases from 3.6 to 11.6 μm with increasing the negative substrate bias voltage from −30 to −300 V. The increase of the CNT forest heights with the applied substrate bias toward larger negative voltages can be as a result of higher ion energies and larger carbon fluxes provided for nanotube growth via the catalyst particles with surfaces being heated up effectively at higher negative substrate bias. In other words, within a certain period of deposition time, large negative bias conditions can accelerate more ion species to bombard the catalyst surfaces with higher kinetic energies due to large momentum gains, leading to effective ion-induced dissociation and much larger production of carbon atoms on the catalyst surface. This can therefore result in a higher catalyst particle temperatures, and consequently in a higher CNT growth rates and increased forest heights. Our results are consistent with the experimental observations reported by Mao et al. [39] and Mehdipour et al. [45], which all demonstrate that high negative bias voltage conditions are suitable for CNT growth.

The application of a high negatively biasing voltage to the substrate during the growth process leads not only to an increase in the CNT terminal height and vertical alignment, but also to the emergence of smaller diameter nanotubes in the forests. A continuous decrease of the average tube diameters with increasing negative substrate bias at levels of −30 V (6.5 ± 0.6 nm) to −300 V (5.1 ± 0.4 nm) can be explained by the sputter-etching of catalyst particles by energetic ion species, resulting in smaller individual particles and CNTs. However, as the substrate bias voltage is increased continuously from −300 to −400 V the CNT forest heights decrease significantly from 11.6 to 0.5 μm, and conversely the average tube diameters are increased from 5.1 ± 0.4 to 8.1 ± 1.3 nm, thereby yielding a relative low density of CNTs. This is possibly because that severe bombardment resulting from over-biasing of the substrate makes the molecular re-sputter from the nanotubes already deposited on the substrate, leading to a lower growth rate and, in turn, a decrease in the terminal height of the CNT forests. Moreover, in the case where the substrate is negatively biased with a voltage up to −400 V, a significant rise of substrate temperature induced by more and stronger bombardment of ions or radicals is expected, which can result in the coalescence of catalyst particles into large agglomerates by an enhanced surface mobility, and consequently nucleate larger diameter CNTs. From these facts, our results demonstrate that the ionic flux and kinetic energy of the growth species are apparently significant factors both in CNT growth rates, terminal forest heights, and average tube diameters during the growth process, care must, however, be taken as over-potential can induce catalyst particle agglomeration/coalescence, and can destroy the original morphology/structure of CNTs.

The influence of the CH_4/H_2 flow ratio on the height and diameter of the CNT forests is depicted in Fig. 4(d). As shown, the upper limit of the CNT forest height, with smallest-diameter nanotubes is obtained at the CH_4/H_2 ratio of 10/50 sccm for 45-min deposition time. By keeping the flow rate of the H_2 constant at 50 sccm, the increase of the CH_4 flow rate (from 10 to 50 sccm) results in the decrease of the CNT forest heights, while the average diameter of the CNTs in the forests increases gradually. We deduce that the height of the CNT forests decreases, but the diameter increases with the flow rate from 10 to 50 sccm of CH_4 due to a faster poisoning of catalyst particles by amorphous carbon on the catalytically active surfaces, caused by the weak etching effects of the hydrogen species in carbon-rich environments [39,41,46]. That is to say, for CH_4 flow rate beyond 10 sccm, an excessive supply of carbon sources causes the accumulation of amorphous carbon that reduces the activity of catalyst particles and the speed of CNT growth. This, in turn, leads to a decrease in the height of grown CNT forests within a certain period of deposition time. Furthermore, formation and larger amount of amorphous carbon deposition on nanotube outer wall surfaces is probably responsible for increment in the average diameter of the CNTs in the forests under conditions of relatively higher CH_4 flow rates of 20–50 sccm [47].

Similarly, when we decrease the CH_4 flow rate from 10 to 1 sccm, we observe that the height of the CNT forests decreases, but increment in the diameter of grown CNTs. In this case, two possible reasons have been proposed for the observed trends. The first reason is probably that under the hydrogen-rich atmosphere (i.e. CH_4/H_2 ratio of 1/50 sccm in our case), the excess of hydrogen supply causes the catalyst particle coarsening (size increase) or deforming during the heating and growth stage, making them to generate large-diameter CNTs and/or less active for nanotube growth [39,41,46,48]. Another may be because that the etching effect during the growth process is perhaps too strong, causing rapid removal of the needed carbon species amount for nanotube formation on the catalyst particles; as a result, carbon deficiency limits the CNT forest height for further growth

[39,41,46]. Further experiments are being performed to investigate the changes in catalyst particle morphology, size, composition, structure, and activity as a function of the CH_4/H_2 ratio in the feed gas mixture and in the plasma. Our results show that the maximum height of the CNT forests with smallest-diameter nanotubes is yielded at the CH_4/H_2 ratio of 10/50 sccm, indicating that an optimal amount of carbon supply exists for efficient CNT growth, and the catalyst particle size is kept small and active throughout the growth process. Therefore, we optimize the growth conditions of the ECRCVD system at the CH_4/H_2 flow ratio of 10/50 sccm during all the experiments.

Finally, we study the effect of the plasma power on the growth of the CNT forests. As shown in Fig. 4(e), the height of the CNT forests increases accordingly with the increase in the forward power (115–750 W) to the top plasma. However, the average diameter of the CNTs in the forests exhibits an opposite trend. It is well known that a higher plasma power can facilitate the dissociation and ionization capability of carbon source gas, giving rise to the production of more carbon radicals and ions [39,49–51]. The increase of carbon supply for nanotube growth at higher plasma powers therefore results in the faster growth of CNTs, and hence forms CNTs with relatively higher yield and longer terminal length [39,49–51]. Meanwhile, the raised plasma temperature resulting from increased power intensity also generates higher temperature on the substrate surface, which can lead to an increased numbers of dissolved and precipitated carbon atoms for significantly enhanced CNT growth rates. Moreover, as plasma power increases, an increase in the amounts of atomic hydrogen through electron impact dissociation of hydrogen feedstock can lead to the enhanced etching effect of atomic hydrogen upon effective removing of amorphous carbon on catalyst surfaces, which is essential for continued growth of CNTs with a well-arranged structure [39,49,50]. As a result, the terminal height of CNT forests can be increased notably when the plasma power is high enough. Further, from the viewpoint of the decreasing nanotube diameter with plasma powers, it is also likely that an increased production of atomic hydrogen does not cause direct damage of the grown CNTs, but may slightly etch nanotube outer surface to result in CNTs with smaller diameters imaged by SEM at high levels of plasma power [52].

From the above discussions it can be inferred that the average height of the CNT forests synthesized on the oxidized Co–Cr–Pt–O catalyst by ECRCVD is strongly influenced by process parameters. However, the CNT forests obtained under different process parameters exhibit only slight variations in the average tube diameters, mostly in the range of about 5.1–9.2 nm measured by high magnification SEM images. The reason behind such small tube diameters and narrow distribution is probably that the synergistic effects of the multi-element catalysis system enhance the overall catalyst particle stability and reliability for being able to maintain a small average size throughout the growth process. A more detailed study is underway to elucidate the exact mechanism responsible for the growth uniformity in our case. Based on the results of the experiments presented, the optimum growth condition is achieved at a substrate preheating temperature of 560 °C (corresponding to ~590 ± 10 °C during the steady growth), a operating pressure of 10^2 Pa, a substrate bias voltage of −300 V, a CH_4/H_2 ratio of 10/50 sccm/sccm, and a plasma power of 750 W for aligned growth of CNTs with the maximum forest height, smallest tube diameter, consistent vertical alignment, as well as less aggregation of tube ends at the ECRCVD process time fixed to 45 min. Accordingly, in the sections below, we will focus on studying the morphological features and structural properties of the CNT forests synthesized under the optimum growth condition.

Fig. 5 show the SEM and TEM images, EDS spectrum, and selected area electron diffraction (SAED) pattern for the

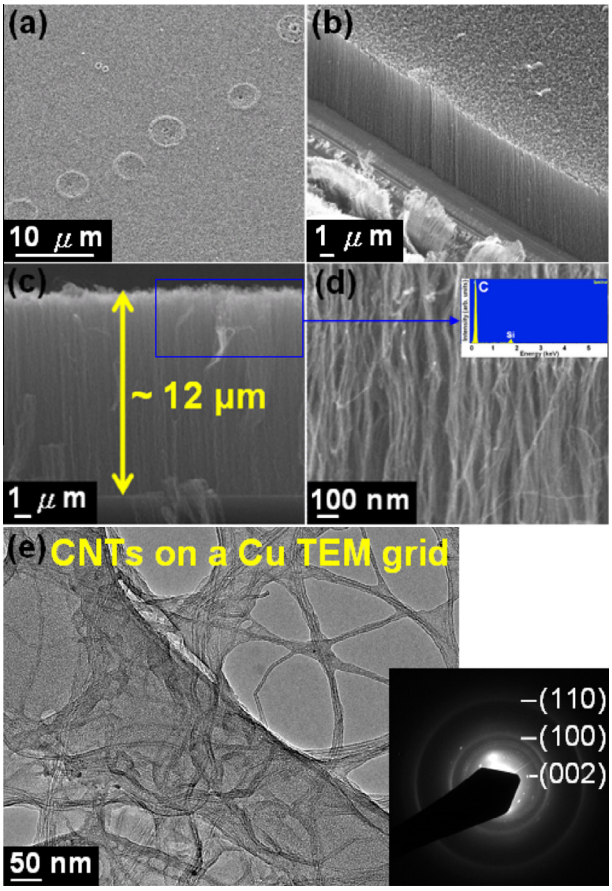

Fig. 5 – Electron microscopy images of the vertically-aligned CNT forests synthesized by ECRCVD using an oxidized Co–Cr–Pt–O catalyst under growth conditions of: a CH_4/H_2 ratio of 10/50 sccm, a substrate preheating temperature of 560 °C, an operating pressure of 10^2 Pa, a substrate bias voltage of −300 V, a plasma power of 750 W, and a deposition time of 45 min. (a) Top-view, (b) side-view, and (c) cross-sectional SEM images showing dense, vertical growth of the CNTs with height uniformity. (d) High magnification SEM image showing the alignment of the CNTs in the forest side-wall. Inset: EDS spectrum of the upper part of the CNT forests, taken from the area marked by the rectangle in (c). (e) Low magnification TEM image of the CNTs placed on a copper TEM grid coated with holy-carbon film. The inset is the corresponding SAED pattern revealing the presence of graphite (002), (100), and (110) reflection rings. (A color version of this figure can be viewed online.)

maximum highest of the CNT forests synthesized via our ECRCVD process of 45 min deposition time, i.e. CH_4–H_2 = 10–50 sccm/560 °C/10^2 Pa/−300 V/750 W. The top-view SEM image of the CNT forests is given in Fig. 5(a), where it can be seen that the substrate surface is widely covered with the dense growth of CNTs. The side-view and the cross-sectional SEM images of the forests given in Fig. 5(b–d) further reveal the vertical growth behavior of the CNTs, where it is evident that the CNTs exhibit a good vertical alignment and have a uniform height of close to 12 μm. The inset of Fig. 5(d) presents the EDS spectrum of the top layer of the as-grown CNT forest samples, taken from the area marked by the rectangle in Fig. 5(c). It reveals that the upper part of the CNT forests consists mainly of carbon element, implying that a large portion of the catalyst particles remains rooted on the substrate surface (base of the CNTs). Consistent with the EDS result, from the SEM observations, we hardly observe catalyst particles clinging at the outer surface of the CNTs, indicating that the as-grown CNT forests possess a clean and smooth surface. This claim is also being verified by the TEM characterization results shown in Fig. 5(e), of which we observe long and thin CNTs, while hardly any catalyst particles are found either inside or outside the CNTs in the TEM imaging area. The SAED pattern (the inset of Fig. 5(e)) taken from the CNTs shows diffraction rings which correspond to graphite (002), (100), and (110) layer planes, respectively.

To investigate the structure of the CNT forests in detail, we then perform HRTEM observation. It is obvious from the HRTEM images displayed in Fig. 6(a and b) that the CNTs obtained are mainly composed of triple-walled graphene structures, with an inner tube diameter mostly in the range of 3.2–3.7 nm and an average interlayer spacing is about 0.34 nm. The results are obtained from several samples, of which more than 100 CNTs are observed for each sample. Note that nanotube diameters measured by TEM are typically less than the limit of what can be accurately obtained from SEM images due to the better resolution of TEM. The HRTEM results indicate that the average diameters of the CNTs in the forests is in good agreement with those of the as-pretreated catalyst particles (3.3–3.9 nm). In other words, the primary catalyst particles can be responsible for the final CNT forest growth in our case. Although a close correlation between average diameters of the catalyst particles and CNTs is observed, a few CNTs with an inner tube diameter somewhat smaller than the initial sizes of the catalyst particles are also found in some of the HRTEM images. Analysis of HRTEM images shown in Fig. 6(c) indicates a triple-walled CNT with an average diameter of ~2.5 nm for inner tubes, which do not clearly correspond to the initial sizes of the as-pretreated catalyst particles. Schäffel et al. [53] indicates the result is probably attributed to the size reduction of some catalyst particles during hydrogen treatment prior to nanotube growth; hence a few CNTs with diameters smaller than those of the particles can be obtained. They further claim that coalescence-induced particle coarsening occurs after CNT nucleation, and therefore produces CNTs with diameter distributions similar to those of the primary catalyst particles. Our experimental results seem to be consistent with Schäffel's findings, confirming that the majority of the as-pretreated catalyst particles nucleate and grow the final CNT forests. In order to further observe the morphological change and elemental compositions of the catalyst particles after the CNT forest growth process, we conduct a cross-sectional TEM study particular emphasis on characterize the samples obtained at the optimum, i.e. the SEM images in Fig. 5(a–d), and results are shown in Fig. 7.

The cross-sectional TEM image in Fig. 7(a) indicates that a high distribution of the catalyst particles remains anchored along the substrate surface implying the predominant growth mechanism is root growth mode. There are a few instances where catalyst fragments seem to either move into the CNT length or distribute randomly within the CNT forests, away from the substrate surface (indicated by red circles in Fig. 7(a)). Moreover, we observe that the catalyst particles residing along the substrate surface are rather irregular and have an increase in the average particle spacing with a wide particle size distribution (~2.1–7.8 nm) compared to those obtained before the CNT forest growth (Fig. 2(a)). Previous reports have documented that catalyst particles can undergo deformations and break apart as a result of being subjected stresses to cause shape change and to yield particles at the tip and base of the carbon tubes before and during nanotube formation [54–56]. Furthermore, a continuous heating process can promote catalyst particle migration/coalescence and Ostwald ripening, thus modifying the final distribution of catalyst particles [53,56–59]. From these facts, we infer that our catalyst particles are probably involved in a series of rearrangement events in the course of the CNT forest growth,

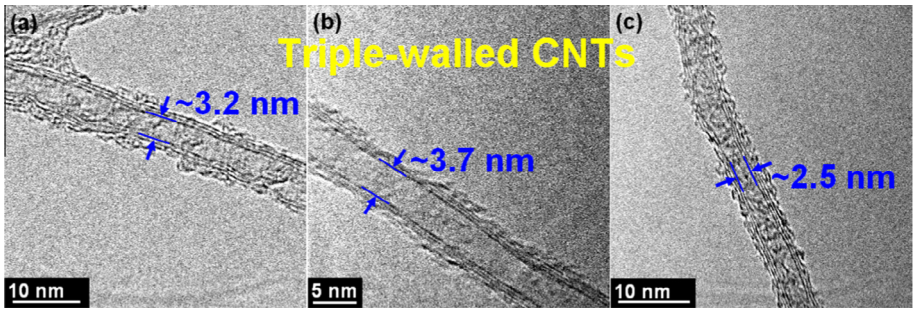

Fig. 6 – HRTEM images of the vertically-aligned CNT forests showing in detail triple-walled graphene structures: (a and b) CNTs with an inner tube diameter mostly in the range of ~3.2–3.7 nm; (c) a CNT with an inner tube diameter of ~2.5 nm somewhat smaller than the initial sizes of the catalyst particles. (A color version of this figure can be viewed online.)

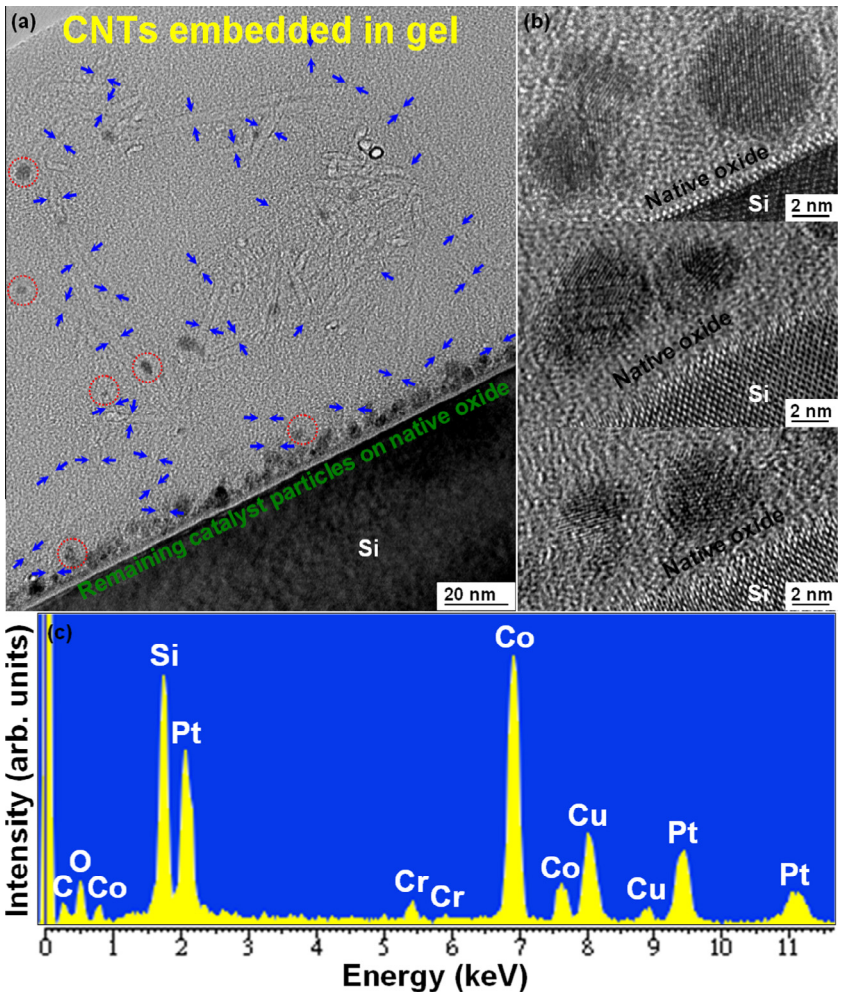

Fig. 7 – (a) Cross-sectional TEM image of the vertically-aligned CNT forests revealing the CNTs with a high distribution of the catalyst particles anchored to the substrate, embedded in gel. (b) Magnified view of the anchored particles taken from three different positions along the substrate surface showing that the catalyst particles maintain crystalline structure after growth has terminated. (c) EDS composition analysis of the catalyst particles residing along the substrate surface. (A color version of this figure can be viewed online.)

which is evidenced by visually apparent changes in the catalyst particle diameter distribution and morphology occur after the CNT forest growth process. Despite a high potentiality of particle re-arrangements in the course of our CNT forest growth, the consistent correlation between primary catalyst particle sizes and final CNT diameters observed indicates that it is the size of the as-pretreated catalyst particles which approximately determines the final diameters of the triple-walled CNTs in our case.

Further HRTEM examination of the anchored catalyst particles at different positions along the substrate surface is presented in Fig. 7(b). The HRTEM images reveal that the catalyst particles remain crystalline with clear lattice planes after growth has terminated. Furthermore, it is interesting to note that no obvious layers of graphene sheets are found around these particles. The features seem crucial because our recent experiments suggest that the successful regrowth of vertically-aligned CNT forests from a recycled catalyst layer is likely tied to the state and active sites of the catalyst. A subsequent paper will be aimed at our ability to recycle the thin oxidized Co–Cr–Pt–O catalyst for multiple CNT forest regrowth cycles, emphasizing the role and activity of the catalyst in each of repeated processes. These samples are further analyzed using EDS to determine if any change in catalyst particle composition occurs after the CNT forest growth process. Fig. 7(c) shows a representative EDS spectrum collected from the catalyst particles residing along the substrate surface. The EDS result reveals a mixed composition of the elements C, O, Co, Cr, Pt, Si, and Cu. The presence of Co, Cr, and Pt indicates that our CNT forest growth process does not cause all of the Co, Cr, and Pt element diffusion/migration to leach out of the as-pretreated catalyst particles, suggesting the retention of co-catalytic functionality within the particles. This fact can be supported by our recent work which demonstrates that after removal of the CNT forests, the substrate is still catalytically active to grow another CNT forests again, with an overall morphology similar to the first growth. The alteration in the concentration and the composition distribution of the mixed multi-element catalyst particles obtained after the CNT forest growth process, however, still need

further experiments to verify. The peaks for C, Si, and Cu come from the CNTs, the Si substrate, and the TEM copper grid, respectively, while the O peak can be attributed to the existence of oxide species in the particles and/or the native oxide on the Si substrate.

Although our understanding of the co-catalytic interactions and mechanisms of the working multi-element oxide catalyst used for the CNT forest growth by the ECRCVD processes is still in a preliminary stage, it is proved on the basis of our experimental results that the Co–Cr–Pt–O material indeed has high and stable catalytic activity, and can act as a new type of catalyst for the synthesis of vertically-aligned CNT forests with a majority of triple-walled tubes. Further studies are clearly needed to investigate the root causes of the synergistic effect in the multi-element catalysis system and to further elucidate the mechanism(s) underlying their catalytic activities.

The graphitization degree and field emission characteristics of the vertically-aligned triple-walled CNT forests are also examined, as shown in Fig. 8. By using Raman spectroscopy, crystallization and defects in the grown CNTs can be analyzed. The Raman spectra in Fig. 8(a) are obtained from the CNT forests synthesized by different experimental runs with the same given growth condition, for which each measurement is averaged over six different regions of the same sample. The peaks around 1340 and 1578 cm^{-1} are attributed to the characteristic D-band (disorder) and G-band (graphite) vibration modes of carbon, respectively [60]. The intensity ratios of the G and D Raman peaks in the spectra (I_G/I_D ratios) of the samples vary in a narrow range from 1.42 to 1.44, indicating a similar degree of wall graphitization among theses CNT forests, even through they are prepared from different experimental runs. Additionally, in order to realize the possible applications of the vertically-aligned triple-walled CNT forests in the area of nanoelectronics, the CNT-forest samples are then electrically characterized in terms of their field emission behavior in a high vacuum system at a pressure of less than 10^{-4} Pa. It is worth mentioning that for obtaining reproducible and stable emission characteristics, high currents are initially generated between the anode and the CNT-forest sample to remove any possible adsorbates on the nanotubes prior to field emission measurements. Fig. 8(b) shows the results of the field emission measurements performed on the CNT forests, averaged over 10 repeated measurements on different regions of the same sample. As shown, the fabricated CNT-forest emitters exhibit a low turn-on electric field (defined as the applied field required for obtaining an emission current density of 10 μA/cm^2) around 2.53–2.60 V/μm and a low threshold field (defined as the applied field required for obtaining an emission current density of 10 mA/cm^2) around 3.67–3.72 V/μm, which are similar to other reported values for as-grown CNTs in forest-like arrays [61–64]. Moreover, a high emission current density of ~110 mA/cm^2 is achieved at the low applied field of 4.5 V/μm, suggesting that the forest-like CNT arrays have potential for use in energy-efficient displays and/or lighting devices. Additionally, it can be found that almost identical current density-applied field (*J–E*) characteristics are obtained, even for the samples from different experimental runs, indicating that the emission from the CNT forests is stable and reproducible. Electron-emission behavior of the CNT-forest samples is further analyzed using Fowler–Nordheim (F–N) model [65] which follows the relation:

$$J = [(1.54 \times 10^{-6})\beta^2 E^2/\varphi] \exp[(-6.38 \times 10^9 \varphi^{3/2})/\beta E] \quad (1)$$

where *J*, β, E, and φ are denoted as the emission current density, the geometric field enhancement factor of the emitter, the applied electric field, and the work function of the emitter, respectively. The inset in Fig. 8(b) is the corresponding F–N plots of ln (J/E^2) vs. 1/*E* from the *J–E* curves of the fabricated CNT-forest emitters. One can see that each plot can be fitted with a linear line shape at higher electric field region, indicating that the CNT forests follow the *F–N* model reasonably well, i.e. the measured currents are generated by field emitted electrons. Moreover, from the *F–N* model, it is possible to obtain the values of β for the CNT forests by using the expression:

$$\beta = -(6.38 \times 10^9) d\varphi^{3/2}/S_{F\text{-}N} \quad (2)$$

where *S* is the slope of the linear region in the *F–N* plots, and *d* is the electrode separation distance, which is 200 μm in this study. Accordingly, by taking the work function of CNTs of ≈5 eV, the β values obtained for the CNT forests are about 2727–2881 from the fitting curves, which is comparable to other reported values on as-grown CNT forests [63,64].

CNTs with a forest morphology are reported to be employed in many applications such as in field emitters, electrochemical and biosensors, supercapacitors, vias and interconnects, or thermal interface materials [1–6]. Consequently, developing

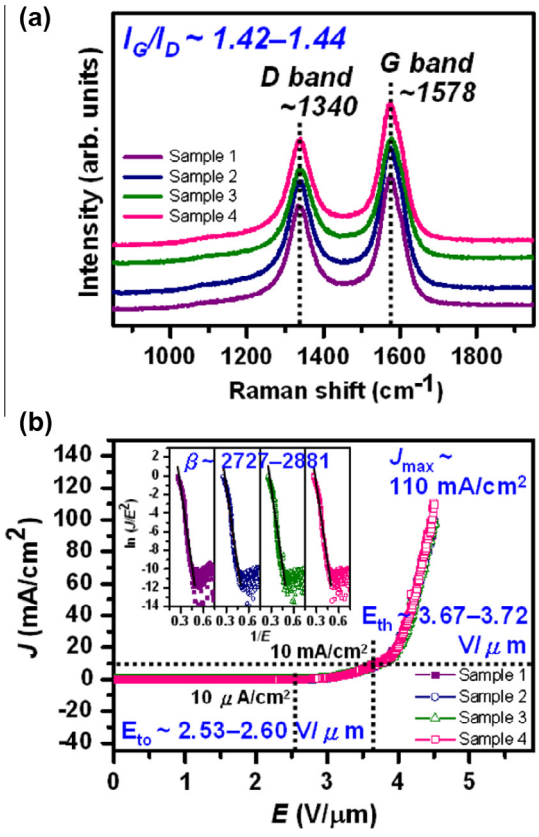

Fig. 8 – (a) Raman spectra and (b) field emission *J–E* curves of the CNT forests synthesized by different experimental runs with the same given growth conditions. The inset in (b) shows corresponding *F–N* plots. (A color version of this figure can be viewed online.)

new catalysts and optimizing growth conditions to synthesize vertically-aligned CNT forests with improved controllability, reproducibility, and homogeneity of the tube structures and size characteristics can be helpful for quite a few applications based on forest-like CNT arrays, it also has broader implications for greatly improving the performance and efficiency of these forests in most applications.

4. Conclusions

In summary, we present in this paper the use of a new oxidized Co–Cr–Pt–O catalyst for synthesizing vertically-aligned triple-walled CNT forests by an ECRCVD sandwich-growth process. It is found that in the multi-element catalysis system, the addition of Cr and Pt as co-catalysts can create a synergistic effect for producing extremely small and uniformly distributed particles (~3.3–3.9 nm in size) after a plasma pretreatment step. XPS core-level analysis reveals that the pretreatment process reduces the metal oxides present in the as-deposited Co–Cr–Pt–O catalyst to their metallic states or to mixed metallic/oxidic states. By adjusting the process parameters, different heights of the CNT forests with slight variations in tube diameters can be prepared. Under an optimal growth condition, the forest height close to 12 μm CNTs is reached, and HRTEM analyses confirm that most of the CNTs have a triple-walled structure, with a clear inner channel mostly of 3.2–3.7 nm inner diameter. Moreover, cross-sectional TEM images clearly reveal that the CNTs grow upwards from the catalyst particles that remain attached to the substrate, indicating a predominantly root growth mode of our CNT forests. Additionally, the field emission measurements are performed on the as-grown CNT forests. The fabricated CNT-forest emitters show a stable and reproducible emission performance with a turn-on electric field of ~2.53 V/μm, a threshold field of ~3.67 V/μm, an emission current density over 100 mA/cm^2 at 4.5 V/μm and a field enhancement factor of ~2881, suggesting promising applications as field emitters. Results of this work provide in-depth understanding of how the newly-developed oxidized Co–Cr–Pt–O catalyst facilitates the production of densely-packed small catalyst particles for vertically-aligned few-walled CNT forest synthesis by ECRCVD, as well as explore the properties and potential applicability of the CNT forests as field emitters. These understanding will help overcome the existing limits to growth of wall-number-selected CNT forests with well-controlled properties effectively for desired applications.

Acknowledgements

This paper was supported by the “Aiming for Top University Program” of the Ministry of Education, Taiwan, Center for Interdisciplinary Science of National Chiao Tung University (NCTU), Taiwan, and the National Science Council of Taiwan under the project number NSC102-2221-E-214-016. The authors acknowledge the facility support provided by the Materials Science and Engineering Department, Center for Nano Science and Technology, and Nano Facility Center of NCTU, and acknowledge valuable discussions with Dr. Wei-Hsiang Wang.

REFERENCES

[1] Chen H, Roy A, Baek JB, Zhu L, Qu J, Dai L. Controlled growth and modification of vertically-aligned carbon nanotubes for multifunctional applications. Mat Sci Eng R 2010;70:63–91 [and references cited therein].
[2] Diao P, Liu Z. Vertically aligned single-walled carbon nanotubes by chemical assembly – methodology, properties, and applications. Adv Mater 2010;22:1–20 [and references cited therein].
[3] Jiang Y, Kozinda A, Chang T, Lin L. Flexible energy storage devices based on carbon nanotube forests with built-in metal electrodes. Sensor Actuat A Phys 2013;195:224–30.
[4] Cole M, Hiralal P, Ying K, Li C, Zhang Y, Teo K, et al. Dry-transfer of aligned multiwalled carbon nanotubes for flexible transparent thin films. J Nanomater 2012;2012. http://dx.doi.org/10.1155/2012/272960. 272960-1–8.
[5] Rivera M, Cole DP, Hahm MG, Reddy ALM, Vajtai R, Ajayan PM, et al. Lightweight carbon nanotube-based structural-energy storage devices for micro unmanned systems. Proc SPIE 2010;8377:837706-1–13.
[6] De Volder MFL, Tawfick SH, Baughman RH, Hart AJ. Carbon nanotubes: present and future commercial applications. Science 2013;339:535–9 [and references cited therein].
[7] Liu Z, Ci L, Kar S, Ajayan PM, Lu JQ. Fabrication and electrical characterization of densified carbon nanotube micropillars for IC interconnection. IEEE Trans Nanotechnol 2009;8:196–203.
[8] Esconjauregui S, Fouquet M, Bayer BC, Ducati C, Smajda R, Hofmann S, et al. Growth of ultrahigh density vertically aligned carbon nanotube forests for interconnects. ACS Nano 2010;4:7431–6.
[9] Fu Y, Nabiollahi N, Wang T, Wang S, Hu Z, Carlberg B, et al. A complete carbon-nanotube-based on-chip cooling solution with very high heat dissipation capacity. Nanotechnology 2012;23:045304-1–7.
[10] Jiang K, Wang J, Li Q, Liu L, Liu C, Fan S. Superaligned carbon nanotube arrays, films, and yarns: a road to applications. Adv Mater 2011;23:1154–61 [and references cited therein].
[11] Zhang M, Fang S, Zakhidov AA, Lee SB, Aliev AE, Williams CD. Strong, transparent, multifunctional, carbon nanotube sheets. Science 2005;309:1215–9 [and references cited therein].
[12] Foroughi J, Spinks GM, Wallace GG, Oh J, Kozlov ME, Fang S. Torsional carbon nanotube artificial muscles. Science 2011;334:494–7.
[13] Aliev AE, Lima MD, Fang S, Baughman RH. Underwater sound generation using carbon nanotube projectors. Nano Lett 2010;10:2374–80.
[14] Jiang K, Li Q, Fan S. Spinning continuous carbon nanotube yarns. Nature 2002;419. 801–801.
[15] Bedewy M, Meshot ER, Hart AJ. Diameter-dependent kinetics of activation and deactivation in carbon nanotube population growth. Carbon 2012;50:5106–16.
[16] Sakurai S, Inaguma M, Futaba DN, Yumura M, Hata K. A fundamental limitation of small diameter single-walled carbon nanotube synthesis—a scaling rule of the carbon nanotube yield with catalyst volume. Materials 2013;6:2633–41.
[17] Lee DH, Kim JE, Han TH, Hwang JW, Jeon S, Choi SY, et al. Versatile carbon hybrid films composed of vertical carbon nanotubes grown on mechanically compliant graphene films. Adv Mater 2010;22:1247–52.
[18] Esconjauregui S, Bayer BC, Fouquet M, Wirth CT, Ducati C, Hofmann S, et al. Growth of high-density vertically aligned arrays of carbon nanotubes by plasma-assisted catalyst pretreatment. Appl Phys Lett 2009;95:173115-1–3.

[19] Terrado E, Tacchini I, Benito AM, Maser WK, Martínez MT. Optimizing catalyst nanoparticle distribution to produce densely-packed carbon nanotube growth. Carbon 2009;47:1989–2001.

[20] Kim HS, Kim B, Lee B, Chung H, Lee CJ, Yoon HG, et al. Synthesis of aligned few-walled carbon nanotubes on conductive substrates. J Phys Chem 2009;113:17983–8.

[21] Choi BH, Yoo H, Kim YB, Lee JH. Effects of Al buffer layer on growth of highly vertically aligned carbon nanotube forests for in situ yarning. Microelectron Eng 2010;87:1500–5.

[22] Zhang Y, Gregoire JM, van Dover RB, Hart AJ. Ethanol-promoted high-yield growth of few-walled carbon nanotubes. J Phys Chem C 2010;114:6389–95.

[23] Moulton K, Morrill NB, Konneker AM, Jensen BD, Vanfleet RR, Allred DD, et al. Effect of iron catalyst thickness on vertically aligned carbon nanotube forest straightness for CNT-MEMS. J Micromech Microeng 2012;22:055004-1–8.

[24] Teblum E, Gofer Y, Pint CL, Nessim GD. Role of catalyst oxidation state in the growth of vertically aligned carbon nanotubes. J Phys Chem C 2012;116:24522–8.

[25] He M, Vasala S, Jiang H, Karppinen M, Kauppinen EI, Niemelä M, et al. Growth and surface engineering of vertically-aligned low-wall-number carbon nanotubes. Carbon 2012;50:4750–64.

[26] Bayer BC, Fouquet M, Blume R, Wirth CT, Weatherup RS, Ogata K, et al. Co-catalytic solid-state reduction applied to carbon nanotube growth. J Phys Chem C 2012;116:1107–13.

[27] Zhang Q, Zhao MQ, Huang JQ, Nie JQ, Wei F. Mass production of aligned carbon nanotube arrays by fluidized bed catalytic chemical vapor deposition. Carbon 2010;48:1196–209.

[28] Moulder JF, Stickle WF, Sobol PE, Bomben KD. Handbook of X-ray photoelectron spectroscopy. Eden Prairie, Minnesota, USA: Perkin-Elmer Corporation; 1992.

[29] Shaijumon MM, Bejoy N, Ramaprabhu S. Catalytic growth of carbon nanotubes over Ni/Cr hydrotalcite-type anionic clay and their hydrogen storage properties. Appl Surf Sci 2005;242:192–8.

[30] Bult JB, Sawyer WG, Ajayan PM, Schadler LS. Passivation oxide controlled selective carbon nanotube growth on metal substrates. Nanotechnology 2009;20:085302-1–7.

[31] Kikukawa T, Nakano T, Shima T, Tominaga J. Rigid bubble pit formation and huge signal enhancement in super-resolution near-field structure disk with platinum-oxide layer. Appl Phys Lett 2002;81:4697–9.

[32] Kim J, Hwang I, Yoon D, Park I, Shin D, Kikukawa T, et al. Super-resolution by elliptical bubble formation with PtO_x and AgInSbTe layers. Appl Phys Lett 2003;83:1701–3.

[33] Tseng JY, Cheng CW, Wang SY, Wu TB, Hsieh KY, Liu R. Memory characteristics of Pt nanocrystals self-assembled from reduction of an embedded PtO_x ultrathin film in metal-oxide-semiconductor structures. Appl Phys Lett 2004;85:2595–7.

[34] Kolobov AV, Wilhelm F, Rogalev A, Shima T, Tominaga J. Thermal decomposition of sputtered thin PtO_x layers used in super-resolution optical disks. Appl Phys Lett 2005;86:121909-1–3.

[35] Kazuma K, Yamakawa Y, Nakano T, Tominaga J. High-speed optical nanofabrication by platinum oxide nano-explosion. J Opt A Pure Appl Opt 2006;8:S139–43.

[36] Zhang L, Li Z, Tan Y, Lolli G, Sakulchaicharoen N, Requejo FG, et al. Influence of a top crust of entangled nanotubes on the structure of vertically aligned forests of single-walled carbon nanotubes. Chem Mater 2006;18:5624–9.

[37] De Volder MFL, Vidaud DO, Meshot ER, Tawfick S, Hart AJ. Self-similar organization of arrays of individual carbon nanotubes and carbon nanotube micropillars. Microelectron Eng 2010;87:1233–8.

[38] Zhang Q, Zhou W, Qian W, Xiang R, Huang J, Wang D, et al. Synchronous growth of vertically aligned carbon nanotubes with pristine stress in the heterogeneous catalysis process. J Phys Chem C 2007;111:14638–43.

[39] Mao M, Bogaerts A. Investigating the plasma chemistry for the synthesis of carbon nanotubes/nanofibres in an inductively coupled plasma-enhanced CVD system: the effect of processing parameters. J Phys D Appl Phys 2010;43:315203-1–15.

[40] Ionescu MI, Zhang Y, Li R, Sun X, Abou-Rachid H, Lussier LS. Hydrogen-free spray pyrolysis chemical vapor deposition method for the carbon nanotube growth: parametric studies. Appl Surf Sci 2011;257:684–9.

[41] Mata D, Amaral M, Fernandes AJS, Oliveira FJ, Costa PMFJ, Silva RF. Self-assembled cones of aligned carbon nanofibers grown on wet-etched Cu foils. Carbon 2011;49:2181–96.

[42] Oda A, Suda Y, Okita A. Numerical analysis of pressure dependence on carbon nanotube growth in CH_4/H_2 plasmas. Thin Solid Films 2008;516:6570–4.

[43] Zhang R, Tsui RK, Tresek J, Rawlett AM, Amlani I, Hopson T, et al. Formation of single-walled carbon nanotubes via reduced-pressure thermal chemical vapor deposition. J Phys Chem B 2003;107:3137–40.

[44] Makris TD, Giorgi L, Giorgi R, Lisi N, Salernitano E. CNT growth on alumina supported nickel catalyst by thermal CVD. Diam Relat Mater 2005;14:815–9.

[45] Mehdipour H, Ostrikov K, Rider AE, Han Z. Heating and plasma sheath effects in low-temperature, plasma-assisted growth of carbon nanofibers. Plasma Process Polym 2011;8:386–400.

[46] Okita A, Suda Y, Oda A, Nakamura J, Ozeki A, Bhattacharyya K, et al. Effects of hydrogen on carbon nanotube formation in CH_4/H_2 plasmas. Carbon 2007;45:1518–26.

[47] Tripathi N, Mishra P, Harsh H, Islam SS. Fine-tuning control on CNT diameter distribution, length and density using thermal CVD growth at atmospheric pressure: an in-depth analysis on the role of flow rate and flow duration of acetylene (C_2H_2) gas. Appl Nanosci 2014. http://dx.doi.org/10.1007/s13204-013-0288-8.

[48] Behr MJ, Gaulding EA, Mkhoyan KA, Aydil ES. Effect of hydrogen on catalyst nanoparticles in carbon nanotube growth. J Appl Phys 2010;108:053303-1–8.

[49] Meyyappan M, Delxeit L, Cassell A, Hash D. Carbon nanotube growth by PECVD: a review. Plasma Sour Sci Technol 2003;12:205–16.

[50] Wu WT, Chen KH, Hsu CM. Growth of carbon nanotubes on cobalt catalyst film using electron cyclotron resonance chemical vapour deposition without thermal heating. Nanotechnology 2006;17:4542–7.

[51] Shin SS, Choi BH, Kim YM, Lee JH, Shin DC. The effects of atmospheric pressure plasma on the synthesis of carbon nanotubes. Microelectron Eng 2009;86:925–8.

[52] Bell MS, Teo KBK, Milne WI. Factors determining properties of multi-walled carbon nanotubes/fibres deposited by PECVD. J Phys D Appl Phys 2007;40:2285–92.

[53] Schäffel F, Kramberger C, Rümmeli MH, Grimm D, Mohn E, Gemming T, et al. Nanoengineered catalyst particles as a key for tailor-made carbon nanotubes. Chem Mater 2007;19:5006–9.

[54] Behr MJ, Mkhoyan KA, Aydil ES. Catalyst rotation, twisting, and bending during multiwall carbon nanotube growth. Carbon 2010;48:3840–5.

[55] Behr MJ, Mkhoyan KA, Aydil ES. Orientation and morphological evolution of catalyst nanoparticles during carbon nanotube growth. ACS Nano 2010;4:5087–94.

[56] Moodley P, Loos J, Niemantsverdriet JW, Thüne PC. Is there a correlation between catalyst particle size and CNT diameter? Carbon 2009;47:2002–13.
[57] Quinton BT, Barnes PN, Varanasi CV, Burke J, Tsao BH, Yost KJ, et al. A comparative study of three different chemical vapor deposition techniques of carbon nanotube growth on diamond films. J Nanomater 2013;2013:356359-1–9. http://dx.doi.org/10.1155/2013/356259.
[58] Shawat E, Mor V, Oakes L, Fleger Y, Pint CL, Nessim GD. What is below the support layer affects carbon nanotube growth: an iron catalyst reservoir yields taller nanotube carpets. Nanoscale 2014;6:1545–51.
[59] Tavasoli A, Anahid S, Nakhaeipour A. Effects of confinement in carbon nanotubes on the performance and lifetime of Fischer–Tropsch iron nano catalysts. Iran J Chem Chem Eng 2010;29:1–12.
[60] Dresselhaus MS, Dresselhaus G, Saito R, Jorio A. Raman spectroscopy of carbon nanotubes. Phys Rep 2005;409:47–99 [and references cited therein].
[61] Wang BB, Zheng K, Shao RW. Comparative study on catalyst-free formation and electron field emission of carbon nanotips and nanotubes grown by chemical vapor deposition. Appl Surf Sci 2013;273:268–72.
[62] Shiratori Y, Noda S. Combinatorial evaluation for field emission properties of carbon nanotubes part II: high growth rate system. J Phys Chem C 2010;114:12938–47.
[63] Lim SX, Chang SL, Cheong FC, Tok ES, Zhang Z, Lim CT, et al. Field emission from decorated carbon nanotube–QDs microstructures with a view to the dominant electron paths. J Phys Chem C 2013;117:14408–17.
[64] Yi W, Yang O. Aligned growth and alignment mechanism of carbon nanotubes by hot filament chemical vapor deposition. Appl Phys A 2010;98:659–69.
[65] Fowler RH, Nordheim L. Electron emission in intense electric fields. Proc R Soc Lond A 1928;119:173–81. http://dx.doi.org/10.1098/rspa.1928.0091.